Li, L., Liu, J., Tseng, M.-L. and Lim, M. K. (2024) Accuracy of IGBT junction temperature prediction: an improved sailfish algorithm to optimize support vector machine. *IEEE Transactions on Power Electronics*, (doi: 10.1109/TPEL.2024.3370690)

Reproduced under a Creative Commons License.
https://creativecommons.org/licenses/by/4.0/

This is the author version of the work. There may be differences between this version and the published version. You are advised to consult the published version if you want to cite from it:
http://doi.org/10.1109/TPEL.2024.3370690

https://eprints.gla.ac.uk/320918/

Deposited on 23 February 2024

Enlighten – Research publications by members of the University of Glasgow
https://eprints.gla.ac.uk

Accuracy of IGBT junction temperature prediction: An improved sailfish algorithm to optimize support vector machine

Lingling Li, Jiaqi Liu, Ming-Lang Tseng and Ming K. Lim

***Abstract*—**This study improves the accuracy of junction temperature prediction, as the IGBT reliability is important for the safe operation of its working system due to junction temperature is limited in its actual performance and reliability. A model based on improved sailfish optimization algorithm to optimize support vector machine (ISFO-SVM) is proposed to solve the problem that the junction temperature prediction accuracy is not high enough. The proposed algorithm is improved by adaptive nonlinear iterative factor, Le'vy flight and differential mutation strategy to optimize the support vector machine internal parameters to predict junction temperature. The results indicate that ISFO-SVM performs better under the same evaluation indexes. The RMSE average value decreased by 67.189%, and the MAPE average value decreased by 63.189%, compared with sailfish optimization algorithm to optimize support vector machine. The prediction error of ISFO-SVM is smaller and the error value is in the [-5℃, 5℃] range accounting for 98.270% of the total test samples. ISFO-SVM has a higher fitting degree than the actual junction temperature and the R2 has reached 99.660%. The model predicts the junction temperature of IGBT modules and provides scientific guidance for system reliability evaluation to maintain safe and stable operation effectively.

***Index Terms*—improved sailfish optimization algorithm; support vector machine; junction temperature prediction; Insulated Gate Bipolar Transistor**

I. INTRODUCTION

Insulated gate bipolar transistor (IGBT) has the advantages of bipolar junction transistor and metal oxide semiconductor field effect transistor that is the most representative product of the third revolution of power electronics technology, and its reliability plays a significant part in the safe operation of application system. IGBT is used in medium and high-power semiconductor devices [1]. Prior studies related reliability problems have been gradually concerned with the wide use of power electronic devices [2] [3]. IGBT produces large switching loss, and result in large junction temperature fluctuation of IGBT module in the working environment of high-frequency and large-power [4]. Generally, the IGBT failure probability is doubled every 10 ℃ rise of ambient temperature [5]. Meanwhile, the junction temperature represents the IGBT actual temperature [6]. This has an sinificant impact on the power converter conversion efficiency and safety. It is necessary to obtain the junction temperature accurately for ensuring the reliable operation of the module. The junction temperature is an important parameter to characterize the reliability of the module.

Especially, the failure rates of different components in power electronic devices are different according to the relevant industrial research statistical data. Fig. 1 shows that the highest failure rate in power electronic devices, accounting for 34% [7]. The power semiconductor device is the weakest link in the whole power electronic device, and its reliability greatly restricts the reliability of the whole device. Literature [8] claimed that the measurement method of IGBT junction temperature has gone through a process from the original measurement method of unpacking the packaging structure, sensor and fiber optic detection technology to the novel mathematical junction temperature calculation models. The development of computational intelligence, intelligent algorithms, machine learning and other technologies are gradually being applied to IGBT junction temperature calculation and prediction [9]. How is the improvement of IGBT junction temperature prediction and uses to evaluating IGBTs' reliability effectively?

Yet, a combined prediction model based on intelligent algorithms and machine learning is established to obtain accurate IGBT junction temperature by studying the working characteristics and failure mechanism, and analyzing the

This study was supported by "Chunhui Program" Collaborative Scientific Research Project of the Ministry of Education of the People's Republic of China [Project No. HZKY20220242] and the S&T Program of Hebei [Project No. 21567605H and No. 225676163GH]. (*Corresponding author: Ming-Lang Tseng*).

Lingling Li and Jiaqi Liu are with State Key Laboratory of Reliability and Intelligence of Electrical Equipment, Hebei University of Technology, Tianjin 300130, China

Lingling Li and Jiaqi Liu are with Key Laboratory of Electromagnetic Field and Electrical Aparatus Reliability of Hebei Province, Hebei University of Technology, Tianjin 300130, China, e-mail: lilingling@.hebut.edu.cn , e-mail: 201921401082@stu.hebut.edu.cn.

Ming-Lang Tseng is with Institute of Innovation and Circular Economy, Asia University, 500 Liufeng Road Wufeng District, Taichung, 41354, Taiwan e-mail: tsengminglang@gmail.com (Corresponding author).

Ming-Lang Tseng is with Department of Medical Research, China Medical University, Taichung, Taiwan

Ming-Lang Tseng is with Department of Industrial Engineering, Khon Kaen University, 40002, Thailand

Ming-Lang Tseng is with Faculty of Economics and Management, University Kebangsaan Malaysia, Malaysia,

Ming K. Lim is with Adam Smith Business School, University of Glasgow, United Kingdom, e-mail: Ming.Lim@glasgow.ac.uk.

relationship between IGBT junction temperature and other parameters[10]. This is significant for the safe and stable operation of power converter devices and the sustainable development of the new energy industry.

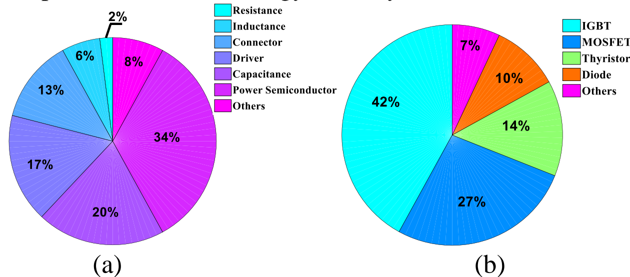

Fig. 1. (a) Failure rate of different devices in power electronic devices; (b) Proportion of power semiconductor devices used

This study establishes an improved sailfish algorithm to optimize support vector machine (ISFO-SVM) prediction model to obtain the junction temperature and evaluates its reliability by analyzing the IGBT junction temperature prediction. The proposed model learns the relationship among the characterization parameters and the actual junction temperature through the combined prediction model training process, and achieve more accurately prediction by optimizing the machine learning model random parameters using intelligent algorithm. The contributions are as follows:

- A high-precision and novel-type prediction model is established based on ISFO-SVM.
- An ISFO with strong global search capabilities and better optimization capabilities is proposed in view of the limitations of SFO.
- The internal parameters of support vector machine (SVM) are optimized by ISFO, and the prediction results obtained by ISFO-SVM are better than other methods comparatively.
- The proposed model improves the prediction accuracy, contributes to effectively evaluating IGBTs' reliability, and improving the reliability of system.

The structure is as follows: the related literature is introduced and analyzed in section II; the test platform is established in section III, and the relationship of relevant parameters is analyzed; the ISFO is proposed and the prediction model based on ISFO-SVM is established in section IV; section V analyzes and verifies the model using experimental data; conclusions and implications are presented in section VI.

II. Literature Review

A. IGBT junction temperature prediction

The methods of obtaining junction temperature are divided into three categories: simulation analysis, experimental measurement, and numerical calculation [11].

The simulation analysis method predicts junction temperature by establishing the model based on the electrical and thermal characteristics [12]. A calculation model based on electrical-thermal coupling is introduced in [13] and the whole radiator was decoupled into several subdivision elements representing different heat dissipation boundary conditions to estimate temperature. However, this method has only been studied on one inverter, so its generalizability may be limited. Literature [14] presented solder fatigue level into the electrical-thermal model, and this model can estimate junction temperature. This model is only validated for one type and lacks universality analysis. Literature [15] presented that an electrothermal management was proposed and based on gate voltage to monitor junction temperature. The transient thermal model of IGBT junction temperature with different physical parameters was simulated by finite element analysis method, and the simulation results were verified. However, the impact of environmental factors on its reliability was not considered that has certain limitations. In sum, the IGBT reliability is evaluated by establishing electrical and thermal models or coupling models to estimate the junction temperature, but the prediction accuracy and generalizability need to be improved.

The experimental measurement methods include contact measurement method and non-contact measurement method [16]. The contact measurement method involves directly assessing the temperature on the surface or within the component using thermal sensors, probe sensors, and similar devices [17]. For example, literature [18] achieved accurate measurement of IGBT current using compact online sensors. Literature [19] used thermistor sensors and temperature observers to monitor changes in the internal temperature of IGBT module. However, the operation steps of the contact measurement method are relatively complex and usually require opening the IGBT package. Compared to contact measurement methods, non-contact measurement methods have simpler operating steps and do not require opening the IGBT package. Instead, devices such as infrared thermal imagers and laser displacement sensors are directly used to measure the surface temperature of the equipment. By analyzing the temperature changes on the surface of the equipment, the temperature of internal components can be inferred. A laser displacement sensor to measure temperature with the different deformation of ceramic substrates was used in [20], and the simulation model was established and verified that the model can accurately predict within the error range of 7.3%. But this method of obtaining data is not very suitable under operating conditions. In summary, the implementation of experimental measurement methods requires a variety of equipment types and high precision requirements for the equipment. Therefore, the procurement and maintenance of equipment require a certain amount of cost.

The numerical calculation methods establish a mapping relationship between electrical parameters and junction temperature, and can to observe the junction temperature by monitoring the status of electrical parameters [21] [22]. Literature [23] elaborated on the relationship between the junction temperature, conduction current, and maximum recovery current to establish a junction temperature monitoring model. Literature [24] conducted a detailed analysis of IGBT fault related parameters and established the relationship between IGBT junction temperature and other parameters by surface fitting the data. Due to the nonlinearity of most parameter changes, the predicted junction temperature values obtained by traditional methods are not accurate enough. The

artificial intelligence methods are derived from numerical calculation techniques and good at learning patterns and regularities within actual data. By extracting features from the data, they delve deeply into the complex relationships between the junction temperature of IGBT and input parameters. Empirical evidence indicates that, compared to traditional numerical calculation methods, artificial intelligence methods exhibit stronger prediction accuracy and generalization capabilities [25].

B. Artificial intelligence in junction temperature prediction

Computer intelligence, machine learning and combined models are developing rapidly to show the advantages of smaller error and higher prediction accuracy [26] [27]. A high-precision IGBT junction temperature online detection model was established by [28], which used step-wise regression method to optimize the model parameters. However, there is a lack of universal validation of the model. The IGBT prediction model based on ant colony algorithm optimized Gaussian process (GP) model was established by [29], compared with the original GP, which improved the prediction accuracy shown by prediction results. However, the complexity of GP is relatively high. Machine learning can discover patterns and rules from large amounts of data, and utilize these rules for prediction and decision-making, thereby improving efficiency and creating more value. Therefore, machine learning can explore the potential connections between the characterization parameters and junction temperature, and utilize these patterns to achieve high-precision prediction.

SVM is a machine learning model with advantages such as efficiency, nonlinear classification ability, robustness, generalization ability, and interpretability, and it has become a powerful tool for dealing with large-scale data regression and complex classification problems [30]. In this study, SVM is selected to characterize the potential relationship between parameters and junction temperature for accurate prediction. However, the internal parameters of SVM greatly influence predictive ability. SFO algorithm is a new intelligent algorithm proposed, and it has been applied to solve many optimization problems [31]. For instance, Literature [32] used the improved SFO to solve the berth allocation problem. In [33], the sigmoid transfer function was introduced into SFO to improve the development capability. Therefore, SFO is used to solve optimization problems, and is selected to optimize the internal parameters in this study.

An ISFO algorithm is proposed to deal with the limitations of SFO and further improve the convergence and optimization performance. A better prediction model based on ISFO-SVM is established. The proposed model achieves iterative optimization of SVM internal parameters through ISFO to improve the prediction accuracy, accelerate the training process, and better handle the nonlinear problem between IGBT junction temperature and other parameters. This method also provides a reference method for the reliability prediction of other devices.

III. EXPERIMENT

A. Establishment of test platform

Power cycle test is a technical means to monitor and investigate the aging and failure process of IGBT power modules throughout their entire lifecycle. As illustrated in **Fig. 2**, the power cycle test can be conducted in two ways. In the constant junction temperature fluctuation (ΔT_j) power cycle aging test, the opening and closing times are brief, enabling the junction temperature to rapidly reach a stable value. However, stabilizing the case temperature proves challenging, and the junction temperature exhibits a large fluctuation amplitude (ΔT_j >100K). This results in significant thermal stress on the chip and aluminum bonding lead components, leading to potential bonding lead failures. Therefore, it is often used to simulate the aging failure of IGBT module bonding leads.

In contrast, the constant case temperature fluctuation (ΔT_c) power cycle accelerated aging test employs longer opening and closing times. This configuration facilitates the stabilization of both the junction temperature and the case temperature of the module. It is presumed that the case temperature is equivalent to the junction temperature, which is conducive to monitoring the junction temperature through case temperature. Furthermore, this test exhibits reduced temperature fluctuations (ΔT_j<80K). This characteristic, in turn, induces failure in the module's solder layer and bonding leads, aligning more closely with the module's failure mechanism. Consequently, this study opted for the constant case temperature fluctuation (ΔT_c) power cycle aging acceleration test to investigate the failure of IGBT.

In the test, the module is heated and cooled by turning it on and off. Upon opening, a large current is applied to the module, causing losses and a rapid increase in junction temperature. The opening time is represented as T_{on}, and once the highest junction temperature, T_{cmax}, is attained, the current is discontinued. Following a closing time, T_{off}, the junction temperature descends to the lowest value, T_{cmin}. This sequence constitutes a complete ΔT_c power cycle.

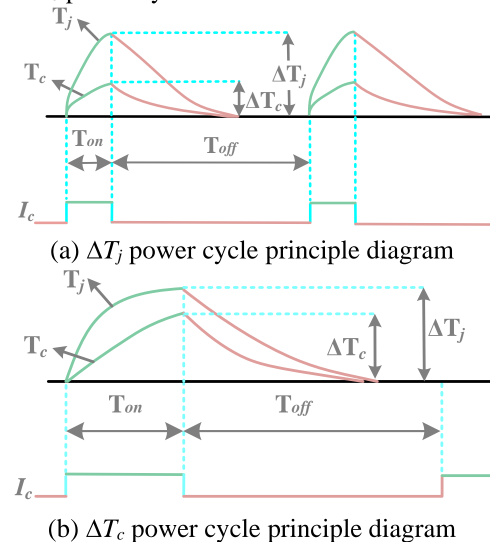

(a) ΔT_j power cycle principle diagram

(b) ΔT_c power cycle principle diagram

Fig. 2. Schematic diagram for power cycle aging test

This study establishes an IGBT power cycle aging accelerated test platform to accelerate aging of IGBT and make T_j change meet the test setting requirements, as shown in **Fig. 3**. In this test, the IGBT model is MMG75SR120B, rated

1200V/75A. The range of junction temperature fluctuation ΔT_j is set to [0℃, 100℃]. The saturation voltage drop fluctuation ΔV_{ce} is increased by 5% as the arbitrary criterion for end of life. According to this standard, the module fails after 6000 test cycles.

The aging test is conducted on the lower arm IGBT for the power module. The IGBT gate of the upper bridge arm is connected to reverse voltage and remains continuously turned off. Regarding the IEC60068-2-14JEDEC standard set for the power cycle test, the basic test procedure is as follows:

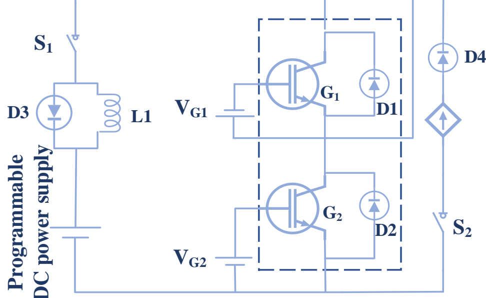

Fig. 3. Platform of IGBT power cycle aging accelerated test

Step 1: Set the initial case temperature (T_c) to 40°C, the output current of the programmable constant current source to 50A, and the gate output drive voltage to 15V. Close the switch S_1, and then power loss is generated by the test module, which causes the T_j and T_c to rise;

Step 2: Monitor the temperature change through the temperature sensor at the bottom of the module. When the maximum case temperature is 90°C, switch off and turn on the air-cooled radiator to quickly cool the IGBT power module to 40°C. One cycle of power aging of case temperature fluctuation is completed;

Step 3: Repeat steps 1 and 2 until the test is stopped when the module is close to the standard end of life criterion. The power cycle test is suspended once every 1000 times. Remove the module and put it into a thermostat for short-term single-pulse test, and record the I_c and V_{ce}.

The rapid rise of the junction temperature results in a big difference with the case temperature, and the accurate internal T_j cannot be obtained through the temperature sensor, due to the self-heating effect caused by the conduction of the module under high current. A small current (≤100mA) is generally applied and the pulse width is less than 0.001s. Under this condition, the module is not to produce self-heating effect, and the case temperature is equivalent to T_j. The single pulse test platform is shown in **Fig. 4.** In **Fig. 4**, the IGBT power module uses a single pulse drive signal to pass a single pulse trigger current to the IGBT through the DSP development board, amplifying circuit and driver. The temperature adjustment range of the thermostat is [0°C, 100°C], and the temperature adjustment interval is 10°C. The setting range of the I_c is [25A, 70A], and the adjustment interval is 5A. The single pulse test steps are as follows:

Step 1: Put the IGBT power module to be tested into a thermostat to adjust the temperature. After the thermostat temperature stabilizes, it is considered that the module has reached thermal equilibrium.

Step 2: Adjust the programmable power supply V_{dc} to achieve the set value of I_c when the thermal equilibrium condition is met. In this test, start with I_c at 25A and increase it by 5A at each current measurement point. At this point, apply a single pulse trigger current to IGBT, and record the data of V_{ce}, T_j and I_c under the corresponding aging times in sequence.

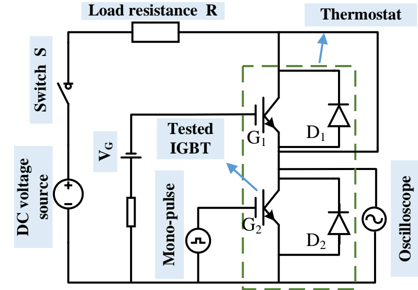

Fig. 4. Platform of IGBT single pulse test

B. Experimental data analysis

Due to the huge amount of data obtained during the IGBT power cycle aging accelerated test platform, this study selected the data of V_{ce}, T_j and I_c under the conditions of the range of I_c is [40A,70A] and the range of T_j is [0℃,100℃] for analysis. After 6000 power cycles of the module, its V_{ce} has increased by about 5.0% compared to the initial value, which has reached the failure standard of the module, and the test is terminated at this time.

To better explore the relationship between V_{ce}, T_j, I_c and aging times, this study conducted a detailed analysis, which focuses on V_{ce} and aging times (**Fig. 5**), V_{ce} and T_j (**Fig. 6**), V_{ce} and I_c (**Fig. 7**).

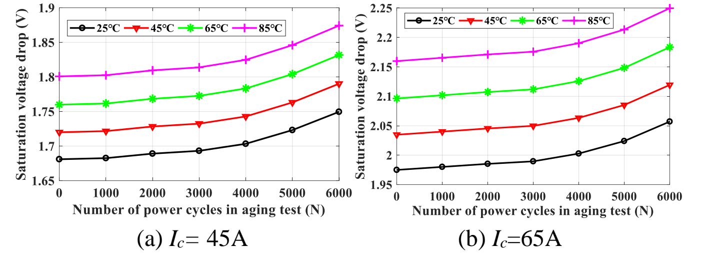

(a) I_c= 45A (b) I_c=65A

Fig. 5. The correlation between the V_{ce} with aging times at I_c

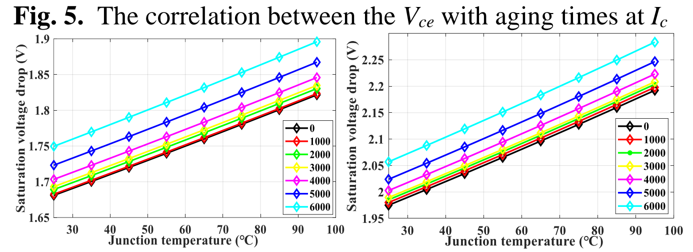

(a) I_c= 45A (b) I_c=65A

Fig. 6. The correlation between the V_{ce} and T_j at I_c

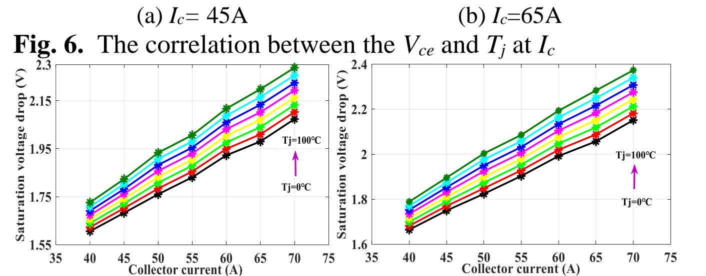

(a) 1000 aging times (b) 6000 aging times

Fig. 7. The correlation between V_{ce} and I_c under aging times

Fig. 5 indicated that under the condition of a certain I_c, as the aging times of power cycles increases, the aging level of the IGBT deepens, and the V_{ce} presents a stepped growth trend. From **Fig. 6**, when the I_c is set to a fixed value, as the aging times increases, the value of V_{ce} also increases. In addition, there is a certain linear correlation between V_{ce} and T_j. Due to experimental equipment testing, the linear relationship is not obvious. **Fig. 7** showed that the I_c is also an important parameter that affects the V_{ce}. The V_{ce} increases with the increase of I_c, and there is a positive correlation between them. As the T_j rises, the relationship curve between the V_{ce} and the I_c moves upward as a whole. It is verified that the T_j has an effect on the saturation voltage drop.

In this study, the V_{ce}, T_j and I_c data obtained under the conditions of the range of I_c is [40A,70A] and the range of T_j is [0℃,100℃] were plotted into a three-dimensional surface graph, as shown in **Fig. 8**. It showed that with the increase of the aging times of power cycles, the relation surface of the relationship between the V_{ce}, T_j and I_c remain unchanged, showing an overall upward trend. In the same aging condition, the V_{ce}, T_j and I_c correlate better with the aging times of power cycles. Therefore, a better relationship between V_{ce}, T_j, I_c and aging times can be used to establish a model based on multi-state parameters for junction temperature prediction.

Based on the above analysis, an IGBT junction temperature prediction model based on ISFO-SVM is established in this study. The relationship between ISFO-SVM and junction temperature characterization can be involved as a learning process. The model achieves high-precision prediction of junction temperature by analyzing and learning the correlation between junction temperature characterization and actual junction temperature.

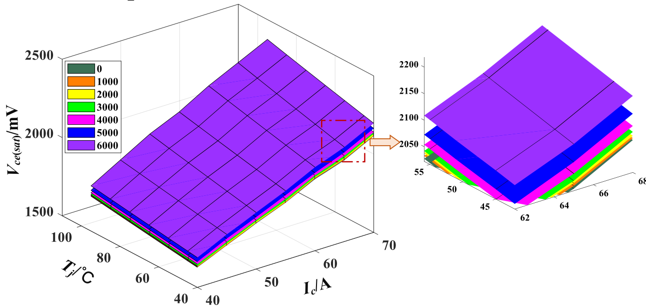

Fig. 8. The correlation curved surface diagram between V_{ce}, T_j and I_c under different aging times

IV. METHOD

A. Support vector machine

SVM is often used for pattern classification and nonlinear regression. In regression prediction analysis, the linear division in high-dimensional space can better deal with small sample problems. The functional relationship is as follows:

$$f(x)=\varepsilon\cdot\phi(x)+b \tag{1}$$

where, ε is the weight coefficient; b is the bias term; f(x) is the prediction value corresponding to sample x.

The objective function of SVM model in the prediction process is as follows:

$$\min\frac{1}{2}\|\varepsilon\|^2+C\sum_{i=1}^{n}(\theta_i+\theta_i^*) \tag{2}$$

$$\begin{cases} y_i-\varepsilon\cdot x_i-b\le\sigma+\theta_i \\ \varepsilon\cdot x_i+b-y_i\le\sigma+\theta_i^* \\ \theta_i\ge 0 \\ \theta_i^*\ge 0 \quad i=1,2\ldots n \end{cases} \tag{3}$$

where, C is the penalty parameter; θ_i and θ_i^* are two relaxation factors; σ is the error between the prediction value and the real value.

IGBT junction temperature is multidimensional and nonlinear. To solve this nonlinear problem, the $K(x_i, x_j)$ is introduced into the SVM model, and the nonlinear optimization problem is expressed as:

$$f(x)=\sum_{i=1}^{n}(\xi_i-\xi_i^*)K(x_i,x_j)+b \tag{4}$$

The expression of the Gaussian kernel function in equation (5).

$$k(x_i,x_j)=\exp\left(-\frac{\|x_i-x_j\|^2}{2\vartheta^2}\right) \tag{5}$$

where, ϑ is the key parameter of the kernel function.

B. Sailfish optimization algorithm

SFO algorithm is a new optimization algorithm proposed in 2019, which is inspired by a group of hunting sailfish.

The initialization includes sailfish and sardine. Among them, the Sailfish population is expressed by X_{SF}, and sardine population is expressed by X_F. SFO consists of two aspects, the following are described in detail.

(a) The search for the best individual position in the sailfish population.

The updated equation of sailfish position is as follows:

$$X_{newSF_i}^{t+1}=X_{eliteSF_i}^{t}-\lambda_i\times\left(r\times\left(\frac{X_{eliteSF_i}^{t}+X_{injuredS_i}^{t}}{2}\right)-X_{oldSF_i}^{t}\right) \tag{6}$$

where, $X_{eliteSF_i}^{t}$ represents the best individual position at the i_{th} iteration; r is random value; $X_{injuredS_i}^{t}$ represents the best individual position in the sardine population at the i_{th} iteration.

The definition of coefficient in equation (6) is shown in equation (7).

$$\lambda_i=2\times r\times PD-PD \tag{7}$$

where, PD represents the density of the prey group, which is described in detail by equation (8).

$$PD=1-\left(\frac{N_{SF}}{N_{SF}+N_S}\right) \tag{8}$$

where, N_{SF} represents the number of sailfish; N_S represents the number of sardines.

(b) The diversity search space of sardine population.

The position update equation of sardine is shown in equation (9).

$$X_{newS_i}^{t}=r\times(X_{eliteSF_i}^{t}-X_{oldS_i}^{t}+AP) \tag{9}$$

where, AP represents the attack strength of the sailfish, which express is shown in equation (10) in detail.

$$AP=A\times(1-2\times t\times e) \tag{10}$$

where, A and e are the control coefficients, which make the attack power of sailfish change linearly from A to 0.

In addition, the number of sardine and their displacement depend on the attack intensity of the sailfish. As mentioned above, sailfish's attack power decreases as time passes. Reducing the attack strength of sailfish can help search agents to converge adaptively.

When $AP>0.5$, that is to say, the attack power of sailfish is strong, equation (9) to update the position of the sardine is used. When $AP<0.5$, the attack power of sailfish is low, and only α and β need to be updated. The range of some positions is defined as follows:

$$\alpha = N_S \times AP \tag{11}$$

$$\beta = d_i \times AP \tag{12}$$

where, d_i is the number of variables at the i_{th} iteration

C. Improved sailfish optimization algorithm

1) To adaptively and dynamically adjust the global and local search ability in the optimization process, an adaptive nonlinear iterative factor is designed to update the position of individuals in the sailfish population. As the number of iterations increases, v_i^t meets the requirements of large value at the initial stage of iteration, fast update speed of search location, slow update speed of search location and fast local convergence. Thus, the global and local search ability of this strategy is better balanced. The mathematical model is shown equation (13).

$$v_i^t = 1 + \sin\left(\frac{\pi \times (2 \times \mathrm{T}_{\max} + t)}{2 \times \mathrm{T}_{\max}}\right) \tag{13}$$

The improvement strategy effectively avoids premature convergence caused by excessive concentration of individuals. With the increase of iterations, the influence of sailfish individual speed update on the search position changes is reduced, which is conducive to the rapid convergence near the optimal value and ensures that the algorithm has a strong local search ability. After introducing v_i^t, the improved position update equation for the i_{th} sailfish and sardine after the iteration of t+1 is as follows in equations (14), (15).

$$X_{newSF_i}^{t+1} = v_i^t \times X_{eliteSF_i}^t - \lambda_i \times (r \times (\frac{X_{eliteSF_i}^t + X_{injuredS_i}^t}{2}) - X_{oldSF_i}^t) \tag{14}$$

$$X_{newS_i}^t = r \times (v_i^t \times X_{eliteSF_t}^t - X_{oldS_t}^t + AP) \tag{15}$$

To improve the randomness of the population, the Le'vy flight strategy is introduced into the algorithm to improve the diversity of the search space. The detailed description of Le'vy flight strategy is shown in equations (16), (17).

$$Le'vy(x) = 0.01 \times \frac{p_1 \times \sigma}{|p_2|^{\frac{1}{\beta}}} \tag{16}$$

where, p_1, p_2 are two random numbers, the value range is [0,1]; β is a constant, β =1.5; σ is calculated as:

$$\sigma = \left(\frac{\Gamma(1+\beta) \times \sin(\frac{\pi\beta}{2})}{\Gamma(\frac{1+\beta}{2}) \times \beta \times 2^{\left(\frac{\beta-1}{2}\right)}}\right)^{1/\beta} \tag{17}$$

where, $\Gamma(x) = (x-1)!$

Currently, the position of sailfish and sardines is updated as:

$$X_{newSF_i}^{t+1} = X_{newSF_i}^t + Le'vy(d) \times X_{newSF_i}^t \tag{18}$$

$$X_{newS_i}^{t+1} = X_{newS_i}^t + Le'vy(d) \times X_{newS_i}^t \tag{19}$$

2) SFO simulates that during the movement of the sailfish hunting, the sailfish can search for prey and the sailfish can attack sardine. At the beginning of iteration, the strong search ability avoids individual aggregation. As the iteration increases, the attack power decreases, and SFO enters the local optimal solution. The algorithm can not completely solve the problems of premature convergence and local optimization, and the optimal result cannot be obtained. The difference mutation strategy is added in each iteration to solve the problem of falling into local optimization after optimization. The equation of difference mutation strategy is as follows:

$$M^{i,t} = x^{k_1,t} + S \times (x^{k_2,t} - x^{k_3,t}) \tag{20}$$

where, $k_1 \neq k_2 \neq k_3$, $x^{k_2,t} - x^{k_3,t}$ is the difference vector; $S \in [0.1, 0.9]$ is the scaling factor; $M^{i,t}$ is the mutation vector of the i_{th} position in the iteration of t.

After obtaining the differential variables, the crossover and selection operation are carried out to select excellent individuals, as shown in equations (21) and (22).

$$u^{i,t} = \begin{cases} M_j^{i,t} & \text{if } j = j0 \ \& \ \mathrm{rand}(0,1) \leq pCR \\ x_j^{i,t} & \text{else} \end{cases} \tag{21}$$

$$x^{i,t+1} = \begin{cases} u^{i,t} & \text{if } f(u^{i,t}) < f(x^{i,t}) \\ x^{i,t} & \text{else} \end{cases} \tag{22}$$

where, $u^{i,t}$ is the cross variable; $j0$ is a random value in the dimension; $pCR \in [0,1]$ is cross probability.

D. The test of algorithm performance

This study uses two groups of standard test functions, as shown in TABLE I. To verify the proposed algorithm, tunicate swarm algorithm (TSA), moth-flame optimization algorithm (MFO), multiverse optimization algorithm (MVO), PSO and chaotic particle swarm optimization algorithm (CPSO) are selected as comparative algorithms, which have been widely recognized and applied. The parameters of TSA are from literature [34]. The parameters of MFO and MVO are from literature [35] and [36]. The parameters of PSO and CPSO are from literature [37]. The parameter settings are shown in TABLE II. In TABLE II, W is the weight coefficient. M is the maximum iterations in PSO and CPSO, C_1 and C_2 are individual learning factors. N is the total number of populations. $a_{\min}$ and $a_{\max}$ are the minimum and maximum convergence coefficients. The remaining parameters are default values. Where, CPSO is a particle swarm optimization algorithm based on chaotic mapping. TSA, MVO and MFO are new swarm intelligence optimization algorithms proposed in recent years, and often selected for solving optimization and regression problems.

To ensure the fairness of the test results, the algorithm is tested on the same platform. The experimental environment of this study is Windows 10 operating system, 8G memory, Intel

Core i7. All experiments are written and run based on MATLAB R2017a. Each algorithm is run 50 times, and the results of final solution are shown in TABLE III.

TABLE III showed that for the $Q_1(x)$ - $Q_4(x)$, under the same number of experiments, the statistical results of ISFO are significantly better than the other six algorithms. For $Q_3(x)$, the ISFO reaches the optimal value 0. The difference between the optimal solution and average value obtained by ISFO is small. The results of ISFO do not fluctuate obviously, showing strong convergence stability and high convergence accuracy. For the $Q_5(x)$ - $Q_7(x)$, ISFO can effectively avoid local extremum solution and has significant advantages in solving multimodal functions. For the multimodal functions $Q_5(x)$ and $Q_7(x)$, the ISFO converges to the function optimal solution 0. For $Q_6(x)$, although the ISFO does not converge to the global optimal value, it converges to 8.88E-16 and maintains stability.

TABLE III showed that ISFO exhibits good advantages in terms of optimization accuracy. However, the optimization time is slightly longer due to introducing the different mutation strategies in the later stage. This study aims to use the ISFO to accurately find the optimal internal parameters of SVM and establish a high-precision IGBT junction temperature prediction model. ISFO with higher optimization capabilities can be used for internal parameter optimization in SVM. More importantly, the method proposed in this study is an offline method. Therefore, the consumption of iteration for optimizing the running time is acceptable.

TABLE I
THE TABLE OF STANDARD TEST FUNCTIONS

Type	Function (Q)	Lower	Upper	Dim	Optimum
Unimodal	$Q_1(x)=\sum_{i=1}^{n} x^2$	-100	100	30	0
	$Q_2(x)=\sum_{i=1}^{n}\lvert x_i\rvert+\prod_{i=1}^{n}\lvert x_i\rvert$	-10	10	30	0
	$Q_3(x)=\sum_{i=1}^{n}(\sum_{j=1}^{i} x_j)^2$	-100	100	30	0
	$Q_4(x)=\max\{\lvert x_i\rvert, 1\le i\le d\}$	-100	100	30	0
Multimodal	$Q_5(x)=\sum_{i=1}^{n}\left[x_i^2-10\cos(2\prod x_i)+10\right]$	-5.12	-5.12	30	0
	$Q_6(x)=-20\exp(-0.2\sqrt{\frac{1}{n}\sum_{i=1}^{n} x_i^2}-\exp(\frac{1}{n}\sum_{i=1}^{n}\cos(2\prod x_i))+20+e$	-32	32	30	0
	$Q_7(x)=\frac{1}{4000}\sum_{i=1}^{n} x_i^2-\prod_{i=1}^{n}\cos(\frac{x_i}{\sqrt{i}})+1$	-600	600	30	0

TABLE II
PARAMETER SETTINGS

Algorithm	Parameter settings
MVO	M=500; N=30
MFO	b=1; M=500; N=30
PSO	C_1=C_2=1.5; W=0.75; M=500; N=30
CPSO	C_1=C_2=1.5; W=0.75; M=500; N=30
TSA	$a_{\min}$=1; $a_{\max}$=4; M=500; N=30
SFO	M=500; N=30
ISFO	M=500; N=30

V. MODEL PREDICTION AND ANALYSIS VERIFICATION

A. Data processing

The experimental data are normalized by mapminmax function to reduce the influence of the fluctuation and non-stationarity of the junction temperature. The principle of normalization of mapminmax function is explained by taking IGBT junction temperature data as an example, and its mathematical expression is as follows:

$$T_{j(scale,i)}=\frac{T_{j(i)}-T_{j(\min)}}{T_{j(\max)}-T_{j(\min)}} \tag{23}$$

where, $T_{j(max)}$ and $T_{j(min)}$ is maximum and minimum values of T_j; $T_{j(i)}$ is the actual value of T_j.

B. Selection of optimization objective function

The mean squared error (MSE) is set as the objective function (F_{obj}), and its expression is:

$$F_{obj}=MSE=\frac{1}{n}\sum_{i=1}^{n}\left(T_i-T_i^{'}\right)^2 \tag{24}$$

where, T_i is the actual value; $T_i^{'}$ is the prediction value.

The fitness function (F_{fit}) of the ISFO in the prediction model is set to have the optimal solution when the function value is the smallest. Then the F_{obj} of the model is the fitness function of the ISFO in the model. Currently, the fitness function is shown in equation (25).

$$F_{fit}=F_{obj}=MSE \tag{25}$$

C. Prediction model of junction temperature based on ISFO-SVM

The ISFO-SVM junction temperature prediction flowchart is shown in **Fig. 9**. The steps are described in detail as follows:

(*a*) The T_j, V_{ce}, I_c and the aging times of IGBT are obtained to make the data set of junction temperature prediction.

(*b*) The V_{ce}, I_c and the aging times as the input data, and T_j as the output data.

(*c*) The data set is divided into training data and test data.

(*d*) Data confusion and data normalization.

(*e*) Set the parameters of ISFO and SVM. The population n

is 30, the maximum iterations t is 500, the dimension D is 2, the value range of the penalty factor C is [0.1, 1200], and the kernel function parameter ϑ is [0.01, 100].

(*f*) ISFO algorithm initialization.

(*g*) Calculate the initial fitness values of all individuals.

(*h*) Start iterative optimization and update the individual position of sailfish according to the position update equation.

(*i*) Calculate the fitness value of individuals, and record the optimal sailfish individual.

(*j*) The difference mutation operation was performed, the position of sailfish in the population was updated, the fitness value was calculated, and the optimal global individual was recorded and updated.

(*k*) Judge whether the iteration gets a better fitness value. If so, run the next step; Otherwise, continue step *h*.

(*l*) Input the optimal parameter combination (C, ϑ) carried by the selected global optimal individual into SVM.

(*m*) The SVM model optimized by ISFO is used to predict the test data of junction temperature.

(*n*) Output the prediction results and inverse normalize the prediction results to obtain the junction temperature prediction value for detailed analysis.

D. Evaluation index

SVM, SFO-ELM, SFO-BP, SFO-SVM and ISFO-SVM prediction models are adopted to compare with ISFO-SVM to demonstrate the better performance of the proposed prediction model. Besides root mean squared error (RMSE), mean absolute percentage error (MAPE) and R-squared (R^2) are also selected as the evaluation indicators of the model.

$$RMSE=\sqrt{\frac{\sum_{i=1}^{Q}(T_i^{'}-T_i)^2}{Q}} \tag{26}$$

$$MAPE=\frac{1}{Q}\left(\sum_{i=1}^{Q}\frac{\left|T_i^{'}-T_i\right|}{T_i}*100\right) \tag{27}$$

$$R^2=\frac{(Q\sum T_i^{'}T_i-\sum T_i^{'}\sum T_i)^2}{(Q\sum(T_i^{'})^2-\sum(T_i^{'})^2)(Q\sum(T_i)^2-\sum(T_i)^2)} \tag{28}$$

where, Q is the number of testing samples; $T_i^{'}$ is the prediction value; T_i is the actual value.

E. Results

There are 2310 sets of data measured through the IGBT power cycle aging accelerated test. To facilitate the establishment of the prediction model with universality and versatility, 386 groups of data from the IGBT power cycle aging accelerated test are selected randomly. The first 70% of the data set is used as training samples, the remaining 30% are used as test samples, which test and verify the effectiveness of the IGBT junction temperature prediction model.

Five prediction models of SVM, SFO-ELM, SFO-BP, SFO-SVM and ISFO-SVM were established by MATLAB, and junction temperature prediction experiments were carried out from the same data. The maximum iterations and the number of populations are set to 500 and 30. The remaining parameters are default value. Each prediction model runs 30 simulation experiments independently. The results of five prediction models of SFO-SVM, ISFO-SVM, SFO-ELM, SFO-BP and SVM are obtained showed in **Fig.10**.

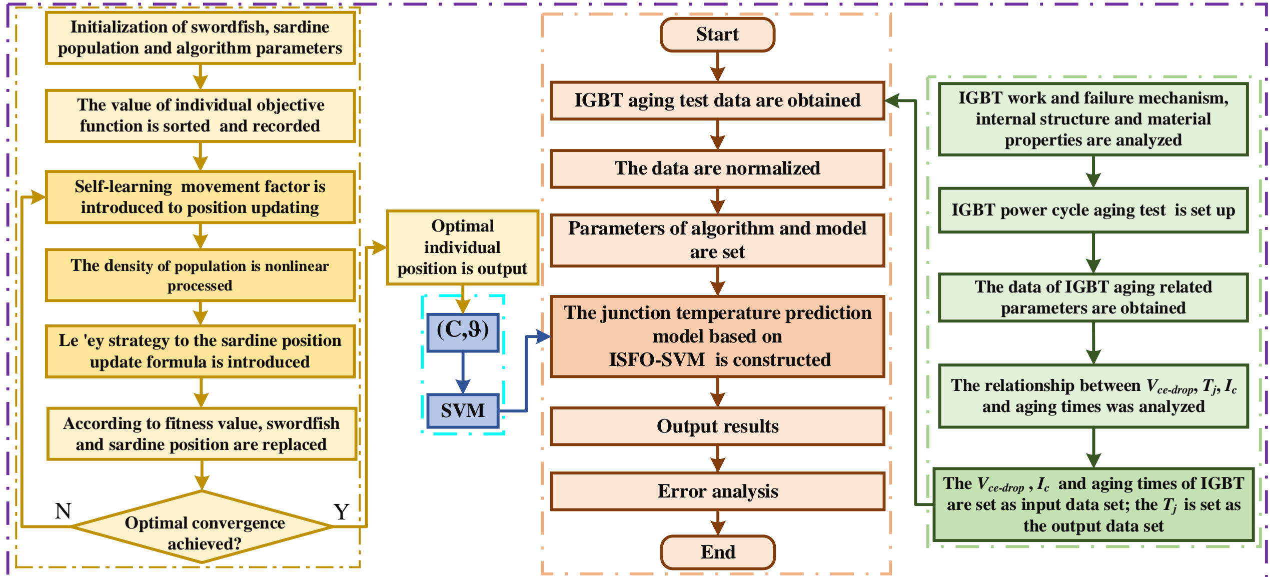

Fig. 9. The flowchart of ISFO-SVM junction temperature prediction model

Fig. 10 showed the comparison between the actual value and the predicted results of the junction temperature. The junction temperature data has great volatility, the prediction errors are quite different although the prediction models can predict the junction temperature. The SFO-SVM has larger errors at a few points. The prediction curve of ISFO-SVM is closest to the actual value. The detailed evaluation indicators of the experimental results are shown in TABLE IV.

In comparing the pros and cons of each model more conveniently, the error curve is obtained to more clearly analyze the magnitude of the prediction errors of the five prediction models in **Fig. 11** and the error histograms in **Fig. 12**.

TABLE IV and **Fig.11** indicated that the RMSE, MAPE and R^2 of ISFO-SVM are better than the other four models, and ISFO-SVM shows better prediction performance and has higher

prediction accuracy. Compared with SFO-SVM, the average RMSE and MAPE of ISFO-SVM have reduced by 67.189% and 63.189%, respectively, and the average R^2 increased by 0.765%. Compared with SFO-ELM and SFO-BP, the average RMSE of ISFO-SVM has reduced by 82.44 % and 74.154%, and the average R^2 also increased by 1.542% and 0.92%. It proves that ISFO-SVM has better performance and prediction accuracy in predicting junction temperature.

TABLE IV
ANALYSIS OF JUNCTION TEMPERATURE PREDICTION AND EVALUATION INDEXES

Model	Index	Minimum	Maximum	Average
SFO-SVM	RMSE/℃	3.312	3.506	3.409
	MAPE/%	6.007	6.225	6.116
	R^2/%	98.752	98.876	98.814
ISFO-SVM	RMSE/℃	1.831	2.247	2.039
	MAPE/%	3.681	4.147	3.914
	R^2/%	99.480	99.660	99.57
SFO-ELM	RMSE/℃	3.41	3.98	3.72
	MAPE/%	6.773	9.56	8.227
	R^2/%	97.71	98.80	98.028
SFO-BP	RMSE/℃	3.22	4.60	3.551
	MAPE/%	4.283	9.924	6.8703
	R^2/%	97.25	98.91	98.65
SVM	RMSE/℃	3.506	3.567	3.5365
	MAPE/%	13.338	13.388	13.363
	R^2/%	98.663	98.693	98.678

In **Fig.12**, the ISFO-SVM has stronger robustness and smaller prediction error for junction temperature prediction. Within the error range of [-2℃, 2℃], the ISFO-SVM covers 67.24% of the total sample points, while the SFO-SVM covers 48.28%. It has been proven that the improvement strategies adopted are effective. Compared to the SFO, ISFO has stronger optimization ability. The ISFO-SVM accounts for 98.27% of the total sample points within the error range of [-5℃, 5℃]. The proportion within this error range is 10.34% and 11.2% higher than SFO-ELM and SFO-BP. The maximum error points appeared in the prediction results of SFO-BP, and the absolute error of the model exceeded 10 ℃, accounting for 1.72%. It can be seen that ISFO can effectively optimize the internal parameters of SVM, thereby enhancing prediction accuracy.

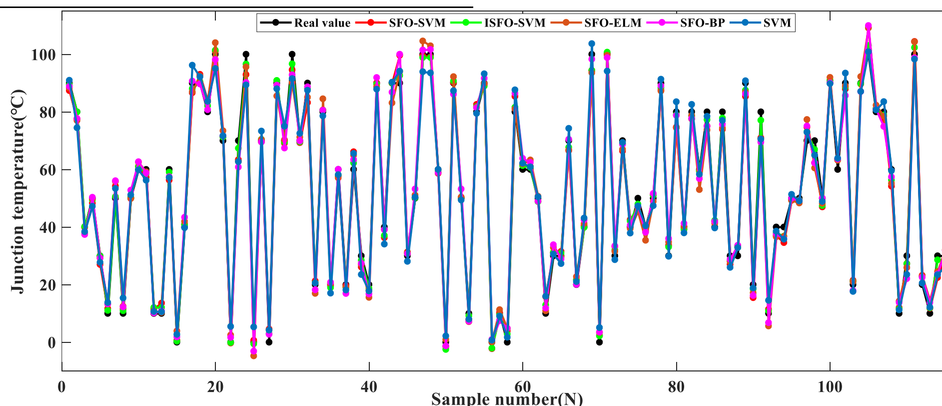

Fig. 10. The prediction results based on five models

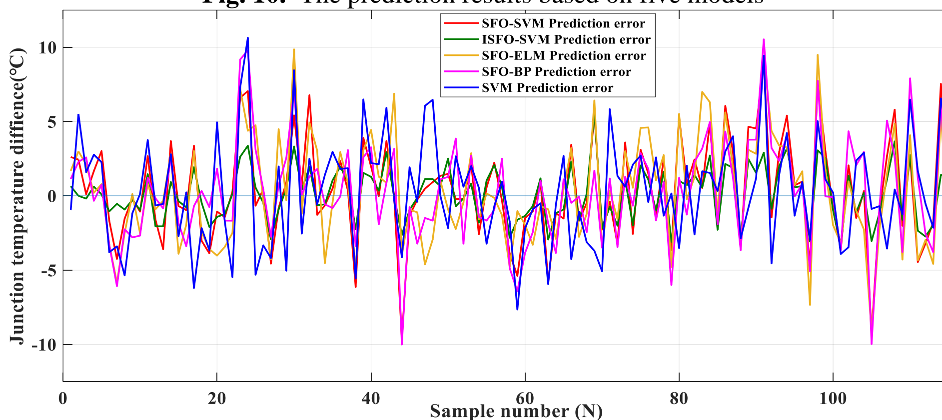

Fig. 11. The error curve comparison chart of the five prediction models

F. Generalizability validation of the proposed model

The universality verification ideas of IGBT junction temperature prediction model based on ISFO-SVM are shown in **Fig. 13**. In addition, based on the type of MMG75SR120B, this study also selected the FGH60N60SMD type and FF300R17ME4 type for verification and analysis , respectively.

(1) Verification of case 1

Conduct experiments on IGBT with FGH60N60SMD type to obtain the required dataset for model validation in this study. And use the process shown in **Fig. 13** for model validation. The results obtained by ISFO-SVM are shown in **Fig. 14**. The statistical results compared to other models showed in TABLE V. From the results, it can be concluded that ISFO-SVM can achieve more accurate prediction of IGBT junction temperature, and its prediction error is smaller compared to

other models.

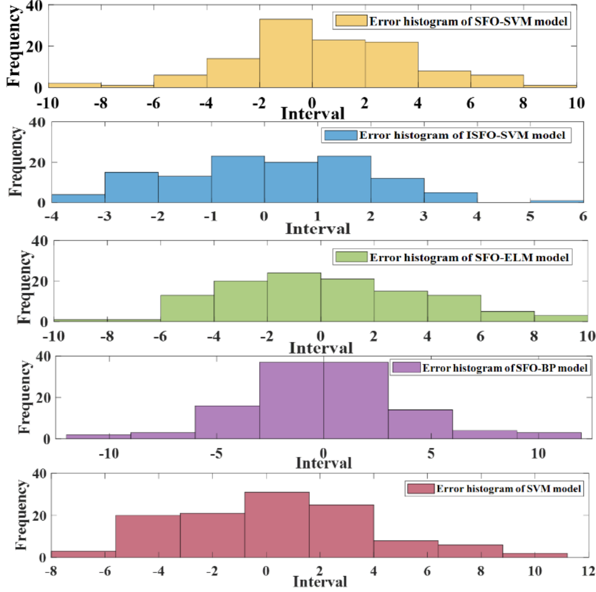

Fig. 12. The error histogram of the five prediction models

TABLE V

STATISTICAL RESULTS OF MODELS WITH FGH60N60SMD

Model	RMSE/℃	MAPE/%	R^2/%
SFO-SVM	5.80	7.83	98.86
ISFO-SVM	5.69	7.87	99.58
SFO-ELM	6.21	8.97	97.57
SFO-BP	6.04	8.57	98.56
SVM	9.07	12.42	96.81

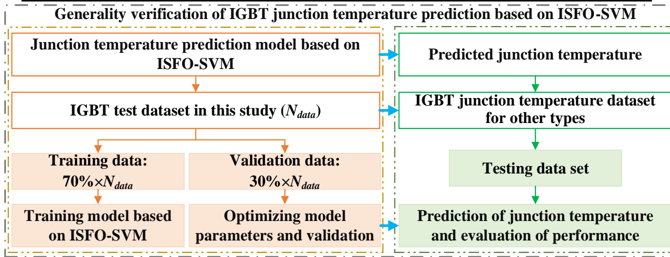

Fig. 13. Verification process of the proposed model

(2) Verification of case 2

To verify the universality of the ISFO-SVM model in multiple aspects, this study fully considered the impact of real-time wind speed on the IGBT junction temperature, and used the FF300R17ME4 IGBT module for simulation to predict the IGBT junction temperature. The prediction results of this model and other models are statistically analyzed, as shown in TABLE VI.

TABLE VI

STATISTICAL RESULTS OF MODELS WITH FF300R17ME4

Model	RMSE/℃	MAPE/%	R^2/%
SFO-SVM	0.326	0.334	99.61
ISFO-SVM	0.251	0.240	99.83
SFO-ELM	0.968	1.311	98.40
SFO-BP	0.623	1.024	98.99
SVM	0.975	1.409	97.94

Fig. 15 indicated that ISFO-SVM can fit the temperature curve well and achieve better prediction results. TABLE VI showed the statistical results of above five models. It showed that ISFO-SVM has the smallest prediction error and the highest coefficient of determination with the actual values.

Through above experiments, it is verified that junction temperature predicted model based on ISFO-SVM can achieve high accuracy, robustness and precision. It is significant for improving the safety, operational efficiency, and lifespan of electrical equipment, and can provide strong support for the maintenance and optimization of IGBT and its systems.

VI. CONCLUDING REMARKS

This study is to achieve high-precision prediction of IGBT junction temperature. And the main findings are as follows:

(1) The data of V_{ce}, I_c, T_j and aging times of IGBT are obtained by aging accelerated test, it is concluded that the other three parameters express the junction temperature by analyzing the data in detail.

(2) An ISFO algorithm is proposed by introducing adaptive nonlinear iteration factor, Le'vy flight and differential mutation strategy. Through the verification of standard test functions, ISFO has better robustness and accuracy.

(3) An ISFO-SVM model used to predict junction temperature is proposed. It is proved that the ISFO-SVM model can better fit the junction temperature by comparing the five models. Moreover, compared with SFO-SVM, the RMSE and MAPE of ISFO-SVM is reduced by 67.189% and 63.189%.

(4) This study conducted experiments on different types of IGBT to validate the universality and versatility of the proposed model based on ISFO-SVM.

IGBT is the central power conversion device and its reliability research has been widely concerned with continuously developing new energy. The scientific research result in this field is to evaluate the reliability of IGBTs from multiple perspectives. High-precision prediction of IGBT junction temperature can effectively assess the remaining useful life and reliability. ISFO-SVM model achieves high precision of IGBT junction temperature prediction, which helps evaluate reliability. This study aims to maintain the reliable operation of IGBT module and its application system. The proposed method is also used in the research of IGBT residual life prediction or the reliability prediction of other devices, which provides valuable scientific method and guidance for investigating high-precision prediction.

There are still some limitations. In future research, the accuracy of prediction model will be enhanced by assigning corresponding weights to different parameters. In addition, this study focuses on developing an accurate method for predicting junction temperature to evaluate IGBT reliability, considering that IGBT junction temperature prediction is an essential topic in its reliability research. Future research can build upon this study to assess the reliability of applications such as power electronics, renewable energy systems, electric vehicles, or industrial automation. Predicting IGBT junction temperature in different application scenarios can help designers and engineers better understand the reliability performance in specific application environments and take appropriate measures to improve system reliability.

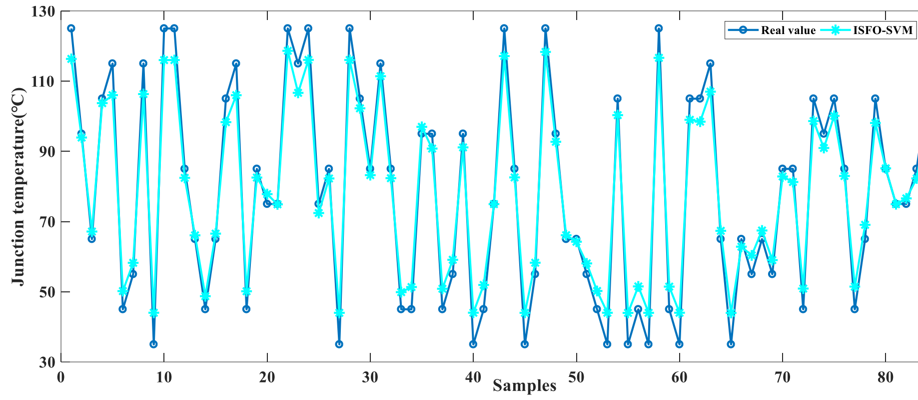

Fig. 14. Junction temperature prediction results with FGH60N60SMD type of IGBT

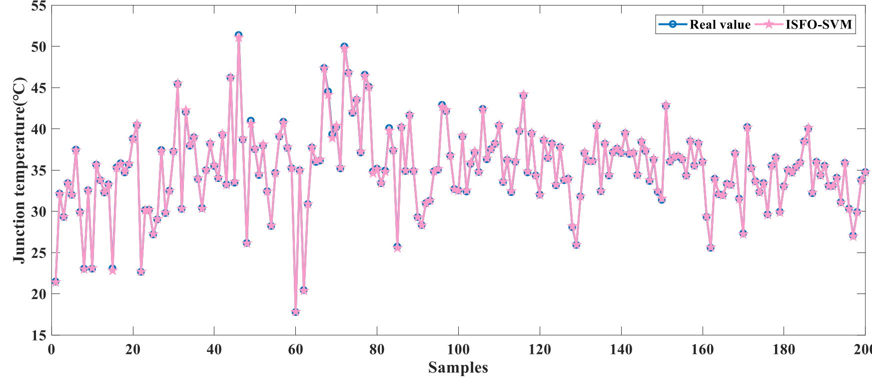

Fig. 15. Junction temperature prediction results with FF300R17ME4 type of IGBT

APPENDIX

TABLE III
THE RESULTS UNDER UNIMODAL TEST FUNCTIONS

Q	Algorithm	Optimum	Worst	Average	$T_m(s)$
$Q_1(x)$	PSO	4.68E-06	2.26E-03	2.16E-04	0.15
	CPSO	2.65E-10	3.82E-07	2.12E-08	0.13
	TSA	2.94E-24	9.26E-20	3.70E-21	0.12
	MVO	0.5688	2.8434	1.2569	0.32
	MFO	0.6972	2.00E+04	2.21E+03	0.28
	SFO	9.70E-19	5.76E-10	8.53E-11	0.44
	ISFO	1.96E-110	2.71E-65	7.14E-67	0.55
$Q_2(x)$	PSO	0.0017	0.2426	0.0333	0.12
	CPSO	5.51E-06	0.0027	2.27E-04	0.14
	TSA	3.07E-15	1.70E-12	1.15E-13	0.14
	MVO	0.3047	9.8143	1.1360	0.28
	MFO	0.1132	70.0521	31.5342	0.15
	SFO	3.45E-07	2.28E-04	3.75E-05	0.46
	ISFO	8.72E-45	4.24E-27	8.77E-29	0.70
$Q_3(x)$	PSO	37.8052	206.337	92.832	0.55
	CPSO	0.4124	7.9412	2.3388	0.50
	TSA	2.59E-08	0.0177	5.32E-04	0.48
	MVO	58.4245	387.670	198.877	0.60
	MFO	4.35E+03	4.81E+04	2.04E+04	0.45
	SFO	9.04E-13	8.26E-07	5.04E-08	1.04
	ISFO	0	8.30E-38	1.67E-39	1.37
$Q_4(x)$	PSO	0.6180	1.9267	1.1474	0.12
	CPSO	0.0831	0.5840	0.2253	0.11
	TSA	0.0096	2.4339	0.4501	0.12
	MVO	0.7901	4.6647	0.0291	0.33
	MFO	49.1851	87.2626	68.3478	0.21
	SFO	5.11E-09	6.14E-06	1.38E-06	0.46
	ISFO	5.20E-45	1.08E-30	2.19E-32	0.51
$Q_5(x)$	PSO	32.9245	87.6035	54.8241	0.11
	CPSO	5.5098	37.9052	23.3663	0.11
	TSA	89.5192	272.585	176.2507	0.15
	MVO	55.3470	191.5869	121.5087	0.34
	MFO	75.7590	255.9174	161.540	0.16
	SFO	5.29E-12	5.17E-05	1.48E-08	0.46
	ISFO	0	0	0	0.67
$Q_6(x)$	PSO	0.0014	2.1201	0.2837	0.11
	CPSO	2.35E-05	1.1551	0.0232	0.11
	TSA	1.88E-12	3.5871	1.3635	0.14
	MVO	0.3557	3.2859	2.0216	0.30
	MFO	0.3120	19.9631	14.3427	0.32
	SFO	2.45E-07	1.86E-05	5.89E-06	0.64
	ISFO	8.88E-16	8.88E-16	8.88E-16	0.66
$Q_7(x)$	PSO	1.92E-06	0.0369	7.66E-03	0.12
	CPSO	5.53E-11	0.1522	0.0278	0.14
	TSA	1.11E-16	0.0890	0.0168	0.25
	MVO	0.6437	1.0177	0.8542	0.31
	MFO	0.2369	91.0419	11.7417	0.33
	SFO	3.94E-14	8.37E-11	9.48-12	0.55
	ISFO	0	0	0	0.64

REFERENCES

1. Yang, Y. Y., Zhang, Q. H. and Zhang. P. J., “A Fast IGBT Junction Temperature Estimation Approach Based on ON-State Voltage Drop,” *IEEE Trans. Ind. Appl.* vol. 57, no. 1, pp. 685-693, Jan 2021.
2. Lai, W., Wang, Z., Hu, Y. L., Chen, M. Y., Xia, H. J., Luo, D., Wei, Y. H., Gao, B. and Chen. Y. G., “Evaluation of IGBT Module Remaining Lifetime in Wind Power Converters Considering Impacts of Failure Location,”

IEEE Trans. Electron Devices. vol. 68, no. 4, pp.1810-1818, Apr 2021.

3. Li, L. L., Fan, X. D., Wu, K. J., Sethanan, K., Tseng, M. L., "Multi-objective distributed generation hierarchical optimal planning in distribution network: Improved beluga whale optimization algorithm," Expert Syst. Appl. vol. 237, Mar 2024, Art. no. 121406.
4. Deng, E. P., Chen, W. N., Heimler, P. and Lutz. J., "Temperature Influence on the Accuracy of the Transient Dual Interface Method for the Junction-to-Case Thermal Resistance Measurement," *IEEE Trans. Power Electron.* vol. 36, no. 7, pp. 7451-7460, Jul 2021.
5. Wang, X. P., Li, Z. G., Yao, F. and Tang, S. X., "Prediction of Chip Solder Fatigue in IGBTs," *IEEJ Trans. Electr. Electron. Eng.* vol. 16, no. 2, pp. 188-198, Feb 2021.
6. Baker, N. and Iannuzzo, F., "The Temperature Dependence of the Flatband Voltage in High-Power IGBTs," *IEEE Trans. Ind. Electron.* vol. 66, no. 7, pp. 5581-5584, Jul 2019.
7. Wang, J. F., Liang, G. S., Qi, L. and Zhang, X. Y., "A More Reliable and Sensitive Overcurrent Detection Method in DC Breaker Surge Current Applications via V-GE as a Desaturation Precursor," *IEEE Trans. Power Electron.* vol. 38, no. 4, pp. 4257-4261. Jan 2023.
8. Zhao, J. Y., An, T., Fang, C., Bie, X. R., Qin, F., Chen, P. and Dai, Y. W., "A Study on the Effect of Microstructure Evolution of the Aluminum Metallization Layer on Its Electrical Performance During Power Cycling," *IEEE Trans. Power Electron*. vol. 34, no. 11, pp. 11036-11045, Nov 2019.
9. Yang, X., Zhang, Y., Wu, X. L. and Liu, G. Y., "Failure Mode Classification of IGBT Modules Under Power Cycling Tests Based on Data-Driven Machine Learning Framework," *IEEE Trans. Power Electron.* vol. 38, no. 12, pp. 16130-16141, Dec 2023.
10. Eleffendi, M. A. and Johnson, C. M., "Application of Kalman Filter to Estimate Junction Temperature in IGBT Power Modules," *IEEE Trans. Power Electron.* vol. 31, no. 2, Feb 2016, Art no. 2418711.
11. Sathik, M. H. M., Pou, J., Prasanth, S., Muthu, V., Simanjorang, R. and Gupta, A. K., "Comparison of IGBT junction temperature measurement and estimation methods-a review," *In 2017 Asian Conference on Energy, Power and Transportation Electrification* (*ACEPT*). *IEEE*, pp. 1-8. Oct 2017.
12. Andresen, M., Schloh, M., Buticchi, G., and Liserre, M., "Computational light junction temperature estimator for active thermal control," *In 2016 IEEE Energy Conversion Congress and Exposition* (*ECCE*). *IEEE*, pp. 1-7, Sep 2016.
13. Chen, H., Yang, J. and Xu, S., "Electrothermal-Based Junction Temperature Estimation Model for Converter of Switched Reluctance Motor Drive System," *IEEE Trans. Ind. Electron.* vol. 67, no. 2, pp. 874-883, Feb 2020.
14. Wei, K., Wang, W., Hu, Z. and Du, M., "Condition monitoring of IGBT modules based on changes of thermal characteristics," *IEEE Access*, vol. 7, Art no. 47525-47534. Apr 2019.
15. Qin, D., Ozkan, G., Edrington, C. and Zhang, Z., "Electrothermal Management Using In-situ Junction Temperature Monitoring for Enhanced Reliability of SiC-Based Power Electronics," *In 2021 IEEE Electric Ship Technologies Symposium* (*ESTS*) *IEEE*, pp. 1-7. 2021.
16. Huang, X. J., Gao, G. A., Hao, J. H.,Zhu, L., Sun, H., Yang, Z. P. and Lin, F., "IGBT Condition Monitoring Drive Circuit Based on Self-Excited Short-Circuit Current," *IEEE Trans. Power Electron.* vol.38, no. 9, pp. 11488-11499, Sep 2023.
17. Ozkan, G., Hoang, P. H., Badr, P. R., Edrington, C. S. and Papari, B., "Real-time thermal management for two-level active rectifier with finite control set model predictive control," *Int. J. Electr. Power Energy Syst.* vol. 131, Art no. 107057. Oct 2021.
18. Guo, W. L., Xiao, G.C. and Wang, L.L., "A Compact Magnetoresistance-Rogowski Hybrid Sensor for Multichip Online Current Sensing in Press-Pack Power Module," *IEEE Trans. Ind. Electron*. Jan 2024. DOI10.1109/TIE.2023.3342316.
19. Xiao, X. C., Ge, X. L., Ke, Q. X., Yong, L. J., Liao, Y. K., Wang, H. M. and Zhang, Y. C., "An Adaptive Temperature Observer for Electrothermal Analysis of IGBT Based on Temperature Characteristics," *IEEE J. Emerg. Sel. Top. Power Electron*. vol. 11, no. 2, pp. 2246-2258, Apr 2023.
20. Jorgensen, A. B., Munk-Nielsen, S. and Uhrenfeldt., C., "Evaluation of in situ Thermomechanical Stress-Strain in Power Modules Using Laser Displacement Sensors," *IEEE Trans. Power Electron.* vol. 36, no. 8, pp. 9411-9418, Aug 2021.
21. Chen, L. Y., Zhang, X. Y., Shi, Y. and Qi, L., "A Novel Mixture-Devices-Based Submodule for MMC by Using Low on-State Voltage IGCT and High di/dt Ability IGBT," *IEEE Trans. Ind. Electron.*vol. 71, no. 3, pp. 2375-2384, Mar 2024.
22. Yang, Y., Zhang, P., "In situ IGBT junction temperature estimation method via a bond wire degradation independent parameter turn-off Vce overshoot," *IEEE Trans. Power Electron.* vol. 68, no. 10, pp. 10118- 10129, Oct. 2021.
23. Yang, K., Song, W., Tang. T., and Chen, T., "Online Monitoring Method of P-I-N Diode Temperature Based on Maximum Recovery Current," *IEEE Trans. Power Electron.* vol. 38, no. 6, pp. 7723-7732, June 2023.
24. Liu, B. Y., Chen, G. L., Lin, H. C., Zhang,W. P. and Liu, J. Q., "Prediction of IGBT junction temperature using improved cuckoo search-based extreme learning machine," *Microelectron. Reliab*. vol. 124, Art no. 114267. Sep 2021.
25. Yang, Y. Y., Ding, X. F. and Zhang, P. J., "A Novel Junction Temperature Estimation Method Independent of Bond Wire Degradation for IGBT," *IEEE Trans. Power Electron.* vol. 38, no. 8, pp. 10256-10268, Aug 2023.

26. Von Rueden, L., Mayer, S., Beckh, K., Georgiev, B., Giesselbach, S., Heese, R., et al., "Informed Machine Learning - A Taxonomy and Survey of Integrating Prior Knowledge into Learning Systems," *IEEE Trans. Knowl. Data Eng*. vol. 35, no. 1, pp. 614-633. Jan 2023.
27. Li, L. L., Ji, B. X., Lim, K. M., Tseng, M. L., "Active distribution network operational optimization problem: A multi-objective tuna swarm optimization model," *Appl. Soft Comput.* vol. 150, Jan 2024, Art no. 111087.
28. Shao, L. F., Hu, Y., Xu, G. Q. and Wang, X. N., "Research on IGBT junction temperature model based on united-parameters," *Energy Rep*. vol. 6, pp. 1416-1423, Dec 2020.
29. Li, L. L., Zhang, X. B., Tseng, M. L. and Zhou, Y. T., "Optimal scale Gaussian process regression model in Insulated Gate Bipolar Transistor remaining life prediction," *Appl. Soft Comput.* vol. 78, pp. 261-273, May 2019.
30. Li, C. B., Lin, S. S., Xu, F. Q., Liu, D. and Liu, J. C., "Short-term wind power prediction based on data mining technology and improved support vector machine method: A case study in Northwest China," *J. Cleaner Prod.* vol. 205, pp. 909-922, Dec 2018.
31. Shadravan, S., Naji, H. R. and Bardsiri, V. K., "The Sailfish Optimizer: A novel nature-inspired metaheuristic algorithm for solving constrained engineering optimization problems," *Eng. Appl. Artif. Intell.* vol. 80, pp. 20-34, Apr 2019.
32. El Hammouti, I., Lajjam, A., El Merouani, M. and Tabaa, Y., "A modified sailfish optimizer to solve dynamic berth allocation problem in conventional container terminal," *Int. J. Ind. Eng. Comput.* vol. 10, no. 4, pp. 491-504, Oct 2019.
33. Ghosh, K. K., Ahmed, S., Singh, P. K., Geem, Z. W. and Sarkar, R., "Improved Binary Sailfish Optimizer Based on Adaptive β-Hill Climbing for Feature Selection," *IEEE Access.* vol. 8, pp. 83548-83560, Apr 2020.
34. Liu, Z. F., Li, L. L., Liu, Y. W., Liu, J. Q., Li, H. Y., Shen, Q., "Dynamic economic emission dispatch considering renewable energy generation: A novel multi-objective optimization approach," *Energy.* vol. 235, Nov 2021, Art. no. 121407.
35. Mirjalili, S., "Moth-flame optimization algorithm: A novel nature-inspired heuristic paradigm," *Knowledge-Based Syst*. vol. 89, pp. 228–249, Nov 2015.
36. Sayed, G. I., Darwish, A. and Hassanien, A. E., "Quantum multiverse optimization algorithm for optimization problems," Neural Comput. Appl. vol. 31, no. 7, pp. 2763–2780, Jul 2019.
37. Tharwat, A., Elhoseny, M., Hassanien, A. E., Gabel, T. and Kumar, A., "Intelligent Bézier curve-based path planning model using Chaotic Particle Swarm Optimization algorithm," *Cluster Comput.* vol 22, no. S2, pp. 4745–4766, Mar 2019.

1